Symmetry breaking and vortex precession in low-swirling annular jets

M. Vanierschot, K. Van Dyck, P. Sas, and E. Van den Bulck

Citation: Physics of Fluids (1994-present) **26**, 105110 (2014); doi: 10.1063/1.4898347
View online: http://dx.doi.org/10.1063/1.4898347
View Table of Contents: http://scitation.aip.org/content/aip/journal/pof2/26/10?ver=pdfcov
Published by the AIP Publishing

PHYSICS OF FLUIDS **26**, 105110 (2014)

Symmetry breaking and vortex precession in low-swirling annular jets

M. Vanierschot,[1,a)] K. Van Dyck,[2] P. Sas,[2] and E. Van den Bulck[2]
[1]*Faculty of Engineering Technology, KU Leuven – University of Leuven, Campus Group T, A. Vesaliusstraat 13, 3000 Leuven, Belgium*
[2]*Department of Mechanical Engineering, KU Leuven – University of Leuven, Celestijnenlaan 300A, 3001 Heverlee, Belgium*

(Received 2 January 2014; accepted 6 October 2014; published online 29 October 2014)

In this paper, the flow dynamics in the wake of a turbulent annular jet is studied using Time-Resolved Stereoscopic Particle Image Velocimetry and Proper Orthogonal Decomposition (POD). In this wake, a central recirculation zone is present which, under certain conditions, shows a low-frequency precessing motion. POD analysis of the measured velocity data shows that at zero swirl, an asymmetry is present in the wake, which motion is random in time. This asymmetry originates from a bifurcation of the flow once a threshold Reynolds number is exceeded. For low-swirl numbers, ranging from $0 < S < 0.12$, the asymmetry is still present and its motion becomes structured into a well defined precession. For $S > 0.12$, the precession is gone and the motion of the asymmetric wake is again random in time, similar like the non-swirling jet. In this paper, a model is developed to describe the influence of swirl on the wake dynamics. The model assumes that perturbations in the inner shear layer near the bluff body wall are convected towards the stagnation point. These perturbations cause a shift in the stagnation points position. This shift is convected back to the inner shear layer through convection in the recirculating flow. The dynamics of this feedback mechanism can be modeled by the nonlinear delayed saturation model. In this paper, the model is adapted for swirling flow and simulations show that good agreement is found with the experiments. © *2014 AIP Publishing LLC*. [http://dx.doi.org/10.1063/1.4898347]

I. INTRODUCTION

Bluff-body combustors are widely used in industrial applications, as they demonstrate several favorable characteristics. First, due to flow separation a region of subatmospheric pressure is created in the immediate wake behind the bluff body causing the flow to recirculate. This central recirculation zone (CRZ) promotes flue-gas recirculation and flame stabilization.[1,2] Second, the bluff body can serve as a fuel injection device in non- or partially premixed combustion, either using cross-flow[3,4] or co-flow injection.[5–7] One widely used type of bluff-body combustor is the annular jet. An annular jet can be seen as the limiting case of a coaxial jet with a velocity ratio (ratio between the velocity of the outer and the inner jet) of infinity. Despite their simple geometrical configuration, coaxial jets exhibit a complex flow field with two shear layers. One in the region between the jet and the environment, called the outer shear layer, and one in the region between the CRZ and the jet, called the inner shear layer.[8,9] These shear layers are characterized by strong anisotropic turbulence. Although the annular jet geometry is axisymmetric, under some conditions the flow exhibits a spontaneous break in symmetry. Del Taglia *et al.*[10,11] reported that for laminar, zero-swirl, incompressible annular jets the break of symmetry is controlled by the Reynolds number and the blockage ratio which can be combined into a state parameter λ. At a certain critical value of the state parameter λ_c, the flow suddenly breaks symmetry.

a)Electronic mail: Maarten.Vanierschot@kuleuven.be

Several authors[12–15] suggest the existence of low space-time frequency oscillations near the stagnation point, located at the end of the CRZ, as velocity measurements show large velocity fluctuations. These studies, however, were unable to identify the spatial aspect of the large fluctuations since the flow field was measured point wise. Patte-Rouland *et al.*[16] did a proper orthogonal decomposition (POD) of the velocity field to study the spatial aspects of the annular-jet wake. Their aim was to decompose the velocity fluctuations into a part induced by the large-scale oscillation and a part attributed to turbulence. Reconstruction of the flow field using the two most energetic POD modes showed that mode 1 corresponds to the motion of the stagnation point, which is correlated with a significant asymmetry of the recirculation zone. Since the 2D-Particle Image Velocimetry (PIV) measurements in the study of Patte-Rouland *et al.*[16] were not time-resolved, no temporal information on this motion was available. For coaxial jets, Rehab *et al.*[17] found that if the velocity ratio was higher than around 8, an unsteady recirculation bubble appeared, which oscillates at a low frequency and high amplitude compared to the mixing-layer instability. They reported a Strouhal number of $St = fD_i/U_0 = 0.035$, where D_i is the diameter of the inner jet and U_o is the mean velocity of the outer jet. Another study by Duwig and Gutmark[18] reports a large-scale oscillation in the recirculation zone of an enclosed ring of jets, which can be regarded as an annular jet broken up into smaller parts. The oscillation is caused by an off-axis rotation of the CRZ and the external recirculation-zone in between the jets and the enclosure. They report a Strouhal number $St_{D_b} = 0.036$, using the diameter D_b of the central recirculation zone as a length scale and the jet bulk velocity as a velocity scale. Vanierschot and Van den Bulck[19] reported an even lower frequency ($St = 2.5 \times 10^{-3}$) in the wake of a turbulent annular jet. The associated oscillation is caused by a tilted CTV (Central Toroidal Vortex) which rotates around the central axis. This precession has a large influence on the flow field as it was shown that near the stagnation point up to 45% of the rms velocity fluctuations can be attributed to the precession of the CTV.

Often swirl is given to annular jet flows to enhance mixing and create large zones of recirculation.[20] At certain swirl numbers, large scale instabilities in the flow field can exist such as vortex breakdown or the precessing vortex core. The dimensionless swirl number S, first proposed by Beér and Chigier,[2] is a measure for the amount of rotation of the flow and is defined as

$$S = \frac{\int_{R_o}^{R_i} 2\pi\rho\overline{UU_\theta}r^2 dr}{R_o \int_{R_i}^{R_o} 2\pi(\rho\overline{U}^2)r dr}, \tag{1}$$

where ρ is the density of the fluid, r is the radius, U the velocity component parallel to the axis x, and U_θ the tangential velocity. The overline represents a time-averaged quantity. R_i is the inner and R_o the outer diameter of the annular jet. This paper investigates experimentally the influence of S on the wake dynamics. The swirl number is restricted to very small numbers ($|S| \leq 0.16$), which is well below the point where classical instabilities like vortex breakdown occur. In these low swirl regimes, data found in literature are scarce.

II. EXPERIMENTAL SETUP

A. Test facility

Experiments were performed on a modified annular-burner setup. A schematic drawing of the test facility is shown in Figs. 1 and 2. Air is supplied by a pressure-controlled source. The flow rate is controlled by an upstream valve combined with a flow rate meter. The air enters a settling chamber through 6 channels to ensure a homogeneous velocity distribution. The settling chamber is disc shaped and has a radius of $11.3R_0$ and a thickness of $3.1D_o$. Before flowing through the annular channel the air passes a swirl generator, which has 12 guide vanes. This swirl generator is an adjustment of the original design by the IFRF[3] with different guide vanes to make it possible to create swirl in both counter- and clockwise direction, which was not possible in the original setup. The swirl number has a maximum magnitude of $|S| = 0.3$ in both rotational directions. The annular channel has an outer diameter D_o equal to 26.8 mm, an inner diameter $D_i = 0.67D_o$, and a length $2.9D_o$. The bluff-body blockage ratio $(D_i/D_o)^2$ is equal to 0.44. The temperature of the air which

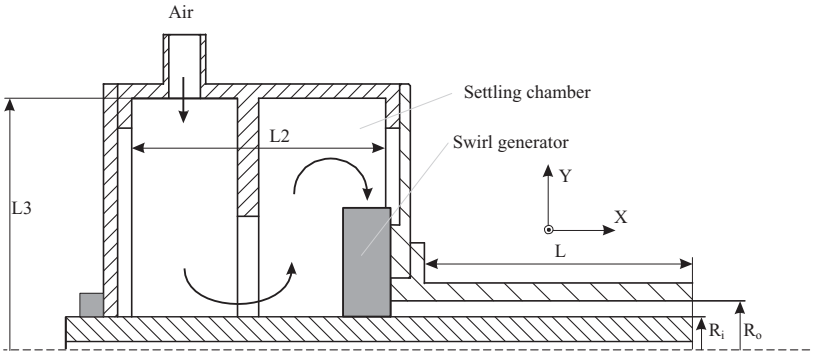

FIG. 1. A cutout drawing of the test facility.

is used to determine the kinematic viscosity ν is measured at a location upstream of the settling chamber by a thermocouple with an accuracy of $\pm 0.1\,^{\circ}$C. Note that at the bluff-body center the channel for co-axial injection of fluid is closed in this study.

B. The PIV system

The flow field is measured using Time-Resolved Stereoscopic PIV. A schematic drawing of the PIV system can be found in Fig. 2. The air coming from the pressure source is seeded with DEHS-oil particles, generated by a Palas AGF 10.0 Liquid Nebulizer, with a diameter between 0.2 and 1 μm. This ensures that velocity fluctuations up to 8 kHz can be followed by the largest particles and 50% of them can follow fluctuations up to 67 kHz.[21]

A planar laser sheet, generated by a NewWave Dual Cavity Nd:YLF Pegasus-PIV laser with a wavelength of 527 nm and a pulse energy of 10 mJ at 1000 Hz, illuminates the seeding particles in the measurement plane. The laser sheet is spanned along the x- and y-axis in a longitudinal measurement plane. The images are recorded using two HighSpeedStar 5 CMOS cameras with a resolution of 1024 $\times$ 1024 pixels and the sample frequency is 125 Hz. The corresponding sampling time scale (8 ms) lies between the integral timescale of the turbulence in the jet ($\approx$ 1 ms) and the time scale corresponding to the precession (0.1–1 s). Therefore, the sampled data are statistically

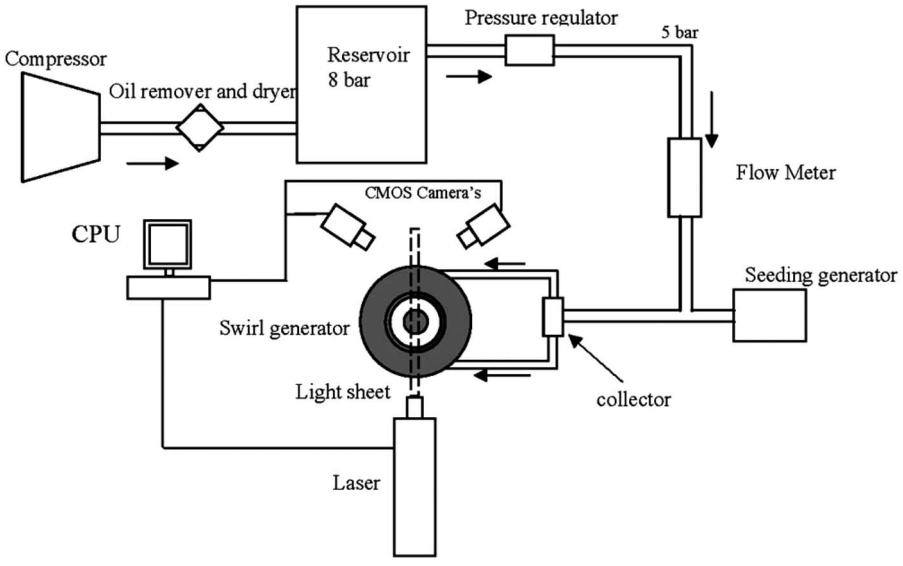

FIG. 2. A schematic drawing of the PIV setup.

independent with respect to the turbulent fluctuations and the time resolution is still sufficiently to resolve the precession. The number of samples N is equal to 1024. This ensures a relative error of around 2% for the mean values of velocity based on a 95% confidence interval. The two cameras are mounted in the forward-scattering direction under an angle of approximately 30° with the laser sheet plane. A Scheimpflug adapter ensures that particles within the light sheet are focused throughout the entire measurement area. The calibration of the PIV system is done using a 3D calibration plate. In order to correct for the misalignment of the laser sheet and the plate, the self-calibration procedure of Wieneke[22] is applied. In this way, a rms fit error smaller than 0.12 px is obtained. The velocity vectors are calculated using the DaVis 7.2.2 software of LaVision GmbH. The images of the two light pulses are recorded on different frames of the cameras and the correlation peak is determined using cross-correlation of these two frames. In order to obtain a good spatial accuracy and a minimization of spurious data, the velocity vectors are calculated iteratively using window deformation. The process starts at an interrogation area of 32×32 px^2 and decreases until a final interrogation area of 12×12 px^2 with 50% overlap. This yields to a spatial resolution of 0.22 mm between two neighboring vectors in both the directions in the measurement plane. Spurious vectors are detected and removed by a median test as first proposed by Westerweek.[23] In this paper, the resulting Cartesian velocity field is denoted by $\overrightarrow{U} = (U, V, W)$ (see Fig. 2 for the definition of the velocity axis). Further data evaluation is done using in-house developed software.

C. Flow conditions and validation

The swirl numbers of the jet studied in this paper are chosen in both rotational directions and range from 0 to 0.16. The Reynolds number Re of the flow is kept constant for each swirl number and is based on the hydraulic diameter $D_h = D_o - D_i$ as length scale, the volume-averaged velocity at the outlet U_0 as velocity scale, and the kinematic viscosity ν at 21 °C equal to 15.3 mm^2/s. This results in a Reynolds number $Re \approx 8600$. As the position of the central rod in the setup is determined by a positioning mechanism (more details can be found in Vanierschot and Van den Bulck[19]), validation of the axisymmetric nature of the flow field is necessary. This validation is done for velocity profiles close to the inlet. These profiles are axisymmetric within measurement accuracy for all swirl numbers studied. Comparing the $\overline{W}$ profiles shows that the swirl generator produces, within measurement accuracy, the same $\overline{W}$ profiles in the two different rotational directions. The swirl number has been determined by numerical integration of Eq. (1). To increase the accuracy, velocity profiles of $\overline{U}$ and $\overline{W}$ are spatially averaged out over different rotational angles. Despite the swirl numbers in this study are very low, this allows an estimation of S within 0.002.

D. Proper orthogonal decomposition

It is widely acknowledged that in turbulent flows large-scale organized motions are present, which are called coherent structures. The study of their dynamics and interaction with each other is important for a better understanding of the flow itself. Different techniques exist to identify the coherent structures, which are often hidden in the incoherent turbulent motions. A few examples of these are (see Adrian *et al.*[24]): the Reynolds-, Galilean-, and LES-decomposition or vortex identification techniques such as the swirl-strength λ_{ci}-criterion. In this paper, an additional technique, the POD (see Berkooz *et al.*[25]), is used. POD projects the velocity field onto an orthonormal base which maximizes the kinetic fluctuation energy for any subset of the base, resulting in a set of modes representing an average spatial description of structures containing most of the energy.[18] Note that the modes do not necessarily have to correspond to coherent structures as they may also correspond to events in the flow that contribute the most, in a statistical sense, to the energy of the flow.[26] An advantage of the method is that it does not need *a priori* knowledge about the flow field of interest. Also one of the main properties is optimality, meaning the decomposition provides the most efficient way to capture the dominant components of an infinite-dimensional process with only finitely, many times a few, modes.[27] It is possible to estimate the velocity field using a truncated number of

modes as

$$\widehat{\vec{U}}(t, \vec{x}) = \overline{\vec{U}}(\vec{x}) + \sum_k a_k(t)\vec{\psi}_k(\vec{x}), \tag{2}$$

where $\widehat{\vec{U}}$ is the estimated velocity field based on a collection of modes with orthonormal base $\vec{\psi}$ and an associated time-coefficient a_k. $\vec{x}$ is the representation of the position vector (x, y, z) and t is the time variable. Note that when all the modes are used to reconstruct the velocity field $\widehat{\vec{U}}$ is equal to $\vec{U}$. The modes are ordered in such way that the kinetic energy contained in mode k is larger than that of mode $k + 1$. The number of snapshots used for the decomposition is equal to 1024. This should be sufficient since Patte-Rouland *et al.*[16] showed that for their decomposition of an annular wake flow with a similar Reynolds number, a number of 400 snapshots is enough to capture the statistics of the first three modes. Also, a previous study by Vanierschot *et al.*[28] shows that POD is able to capture the flow dynamics of the annular wake and hence is suitable for this study. Moreover, only the first two modes are needed in the reconstruction.

III. RESULTS AND DISCUSSION

A. Flow structures for $S \approx 0$

Figure 3 shows the in-plane velocity vectors of the annular jet at $|S| = 0$. As can be seen on the figure, the wake behind the central tube is slightly asymmetric. This symmetry breaking of annular jets is also reported in literature by Del Taglia *et al.*[10] In their numerical study, symmetry breaking occurred even for symmetric boundary conditions. A simple mechanism for the transition to asymmetry is proposed in another paper by Del Taglia *et al.*[11] They stated that perturbations in the inner shear layer near the nozzle exit are convected towards the stagnation point and cause there a shift in location. In order to study the large scale motions of the wake, a POD decomposition of the wake is performed. Fig. 4 shows the first two spatial modes ($\vec{\psi}_1$ and $\vec{\psi}_2$) and their influence on the flow field. With respect to the third and higher eigenmodes no clear conclusions can be drawn of their influence on the wake motion. The first two spatial eigenmodes are very similar to the ones found in the POD analyses by Patte-Rouland *et al.*[16] and Vanierschot *et al.*[28] For $\vec{\psi}_1$ the ratio of the maximal in-plane vector over the maximal out-of-plane vector is equal to approximately 2.6, while for the second spatial eigenmode this ratio is approximately the same but inversed. Consequently, $\vec{\psi}_1$ is primarily composed of in-plane motion, while $\vec{\psi}_2$ especially has an out-of-plane influence. Also mode 2 is a rotation of mode 1 around the central axis of the jet by $\pi/2$ radians. To study the effect of each eigenmode on the flow field, the wakes motion is reconstructed with selected eigenmodes using Eq. (2). The effect of the first eigenmode on the flow field can be seen in

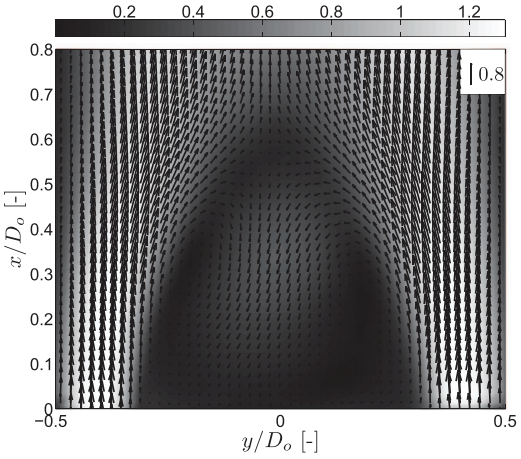

FIG. 3. Velocity vectors of the non-swirling jet. The vectors are scaled with U_0. Colored according to magnitude.

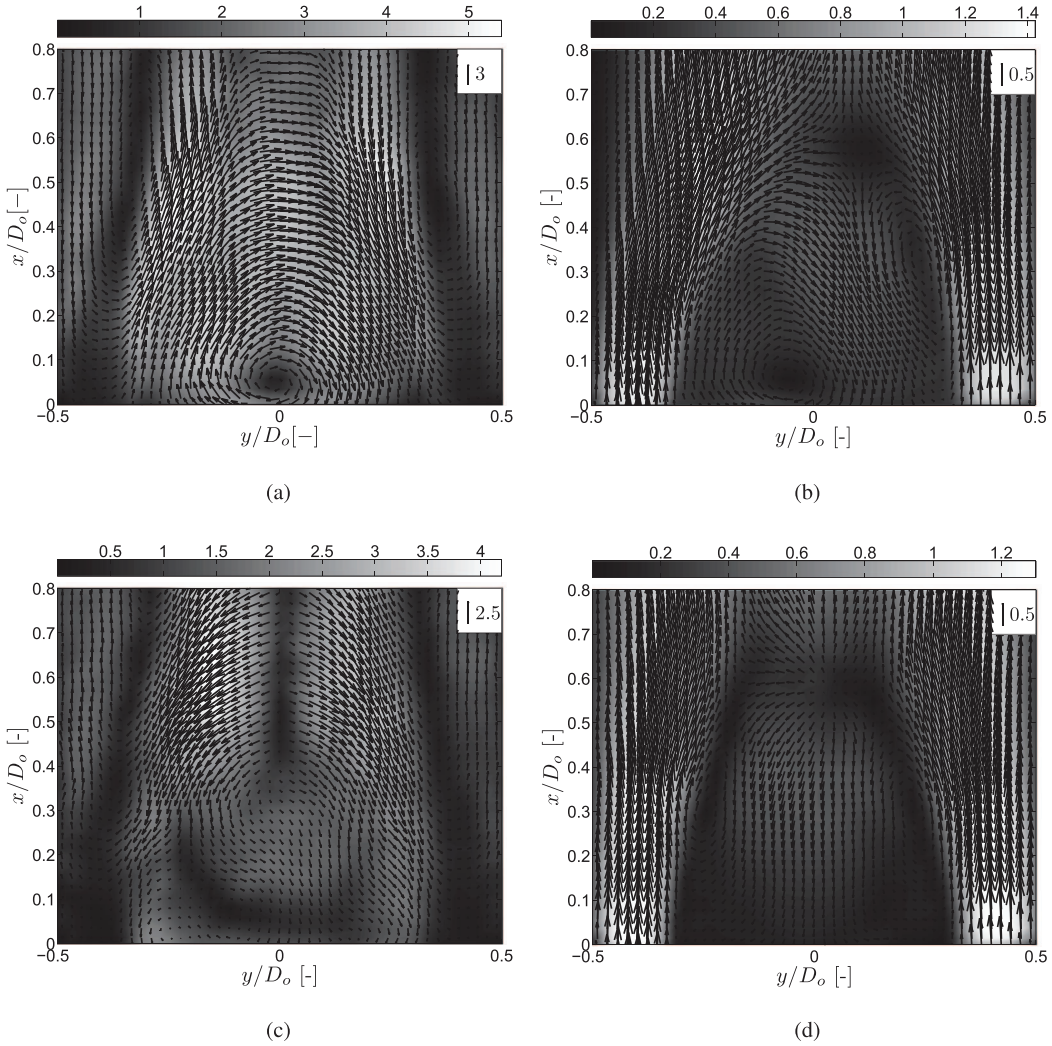

FIG. 4. Effect of the first two eigenmodes $a_1\overrightarrow{\psi}_1/U_0$ and $a_2\overrightarrow{\psi}_2/U_0$ on the flow field ($|S| = 0$). Data from a longitudinal measurement plane. Colored according to magnitude. Note: only one in four vectors is shown. (a) $\overrightarrow{\psi}_1/U_0$, (b)$\overrightarrow{\overline{U}}/U_0 + \max_{\forall t}(a_1)\overrightarrow{\psi}_1/U_0$, (c) $\overrightarrow{\psi}_2/U_0$, (d) $\overrightarrow{\overline{U}}/U_0 + \max_{\forall t}(a_2)\overrightarrow{\psi}_2/U_0$.

Fig. 4(b), where the first mode multiplied by the maximum of the time coefficient a_1 is added to the time-averaged velocity-field. Clearly, the first eigenmode is responsible for a significant asymmetry in the recirculation zone, as the recirculation flow strongly points towards the right-hand side (see also Patte-Rouland *et al.*[16] and Vanierschot and Van den Bulck[19]) The reconstruction of the flow field with only the second mode is shown in Fig. 4(d). As can be seen, mode 2 describes an out-of-plane motion of the wake, especially near the stagnation point.

The temporal reconstructions coefficients a_1 and a_2 are shown in Figs. 5(a) and 5(b). These coefficients are filtered in time with a low pass filter to remove the high frequency turbulent fluctuations. Examination of the time coefficients a_1 and a_2 shows that fluctuations with a large timescale are present and the amplitude having both negative and positive values. Cross correlation of a_1 and a_2 shows that they are essentially uncorrelated. Looking at the time spectra of the coefficients no clear peak can be defined. In order to reveal the time characteristics, Figs. 5(c) and 5(d) show the wavelet analyses of a_1 and a_2. These figures show fluctuations which have dimensionless frequencies in the order of $St \sim 0.002 - 0.01$, which is much lower than Strouhal numbers associated with shear layer instabilities. Several authors have also reported on these large scale fluctuations near the

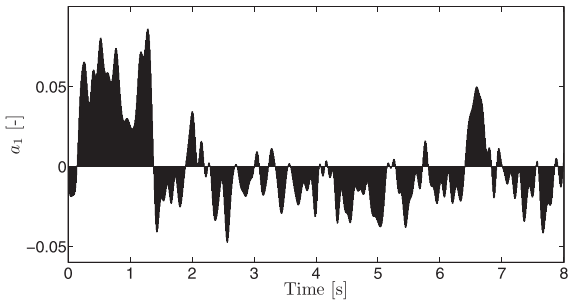

(a)

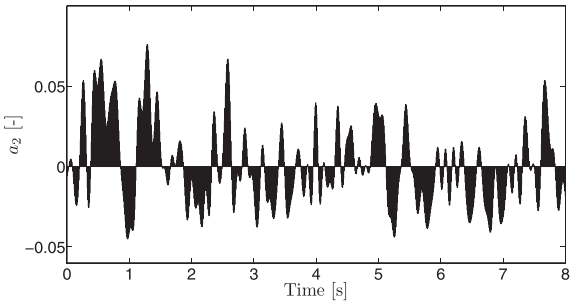

(b)

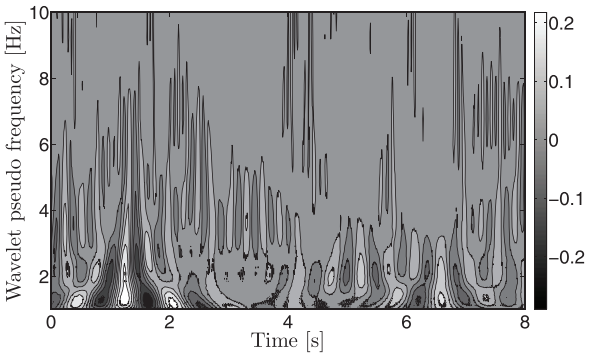

(c)

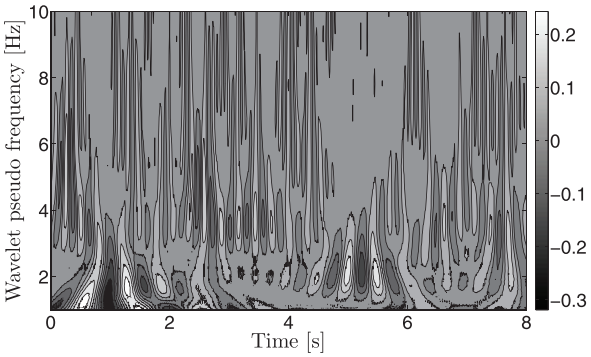

(d)

FIG. 5. Temporal reconstruction coefficients and their wavelet analysis. A Morlet wavelet is used in the decomposition. (a) First mode temporal reconstruction coefficient a_1, (b) second mode temporal reconstruction coefficient a_2, (c) wavelet decomposition of the first temporal coefficient a_1, (d) wavelet decomposition of the second temporal coefficient a_2.

stagnation point.[12–15] However, no clear harmonic oscillation can be found which implies that the CRZ asymmetry has a quasi-random orientation in time and there is no periodic motion.

The mechanism of disturbances proposed by Del Taglia *et al.*[11] is unable to explain the low frequency motions of the stagnation point since the frequencies associated with their convective timescales are much higher. Therefore, we suggest a model which involves feedback from the stagnation point back to the inner shear layer. The mechanism works in the following way. Instabilities in the inner shear layer are convected towards the stagnation point, causing there a shift in location. This shift in location is convected back to the inner shear layer by the recirculating flow in the wake vortex. This feedback process has a time delay τ which is the time necessary for disturbances to be convected form the stagnation point to the inner shear layer. For the jet in our study, the convective feedback time can be approximately calculated from the mean velocity profile and is approximately equal to 5.5 ms, giving a dimensionless delay time (scaled with the jet velocity and bluff body diameter) in the order of $\tau \approx 3$.

A general dynamical model to analyze this feedback mechanism is based on the equation of Landau for weakly nonlinear instabilities and was first introduced by Villermaux.[29] This equation describes the time evolution of a relative amplitude $A(t)$, where $A(t) \sim (aX_s - \delta X_s)/X_s$, with X_s the position of the stagnation point and a a proportionality constant. The dynamic equation for $A(t)$ is given by

$$\frac{d}{dt}A(t) = \sigma A(t) - \mu |A(t-\tau)|^2 A(t), \tag{3}$$

where σ is the perturbation growth rate, μ sets the amplitude, and τ is the convective feedback time. The nonlinear term on the left hand side prevents unphysical growth of the amplitude at long times. This nonlinear saturation is effective after a time lag τ and hence the model is called the nonlinear delayed saturation model or NLDS. More information regarding the NLDS model can be found in Villermaux *et al.*[29,30] Equation (3) has no steady state amplitude if $\sigma\tau > \pi/4$. The period of oscillation T can be approximated by

$$T \approx \tau \left(2 + \frac{(1-\beta)^2}{1-\beta^2} e^{2(1-\beta^2)\sigma\tau}\right), \tag{4}$$

with $\beta \approx 0.45$. For an axisymmetric shear layer, the dimensionless growth rate of the perturbations depends on the wave number, but is generally in the order of one.[31,32] The zero swirling jet has a value of $\sigma\tau \sim 3$, which is in the unstable regime of Eq. (3). Figure 6 shows the numerical calculation of Eq. (3) for $\sigma\tau = 3$. More details regarding the algorithm can be found in Shampine and Thompson.[33] Although the frequency of oscillation $1/T$ is well defined, the direction of the amplitude becomes highly dependent on the initial conditions and shows chaotic behavior. The same can be found in the wavelet analysis in Fig. 9. Higher frequency oscillations corresponding to $1/T$ are superimposed on an amplitude which changes sign randomly in time (Figs. 5(a) and 5(b)). A close relation exists between the amplitude of the convected disturbances and the temporal reconstruction coefficients of the POD analysis even if turbulence is not taken into account in Eq. (3). Moreover, looking at the frequency spectrum of $A(t)$ (Fig. 6(b)) also shows no clear frequency peak, but several small peaks at low Strouhal numbers, which is also observed in the experiments. Also, the frequencies are in the same order of magnitude.

B. Flow structures for $0 < S < 0.12$

Figure 7 shows the velocity vectors of a low swirling jet with swirl number $|S| = 0.015$. In contrast to the non-swirling flow, the wake behind the central tube is symmetric. Apart from that the wake is very similar compared to the non-swirling jet and these very low swirl numbers hardly change the structure of wake. The spatial eigenmodes of the POD analysis of the swirling jet, shown in Fig. 8, are almost identical to the ones found in the non-swirling jet. The first mode ($\vec{\psi}_1$) can be found in Fig. 8(a). This spatial structure represents the motion of the stagnation point in the measurement plane and is responsible for the asymmetry in the wake. Comparison with Fig. 4(a) shows they are very similar. The second mode ($\vec{\psi}_2$) can be found in Fig. 8(c). This spatial structure

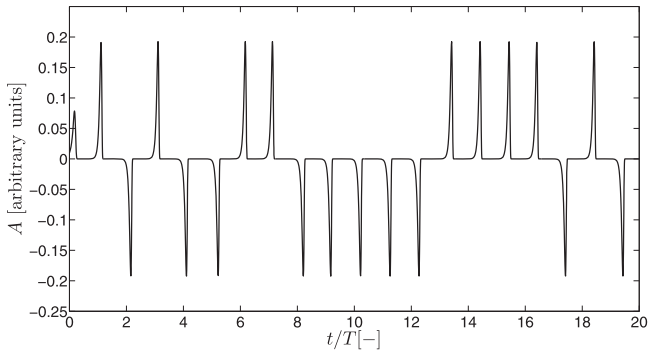

(a)

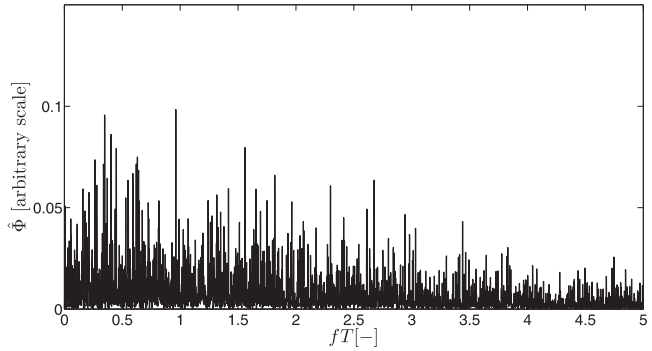

(b)

FIG. 6. Results of the numerical simulation of Eq. (3). The dimensionless feedback time $\tau = 3$, $\sigma\tau = 3$, and $\mu = 4000\sigma$. (a) Amplitude $A(t)$ as a function of the dimensionless time scaled with T. The amplitude is plotted in arbitrary units, (b) frequency spectrum of $A(t)$.

represents the out-of-plane motion of the stagnation point. Comparison with Fig. 4(c) shows this mode is very similar to the corresponding mode of the non-swirling jet. Like for the non-swirling jet, no clear conclusions can be drawn of the influence of the third and higher modes on the wake motion. POD analysis of the flow structures at other swirl numbers (not shown here) shows that these are identical to $|S| = 0.015$ in the swirl number range $0 < S < 0.12$.

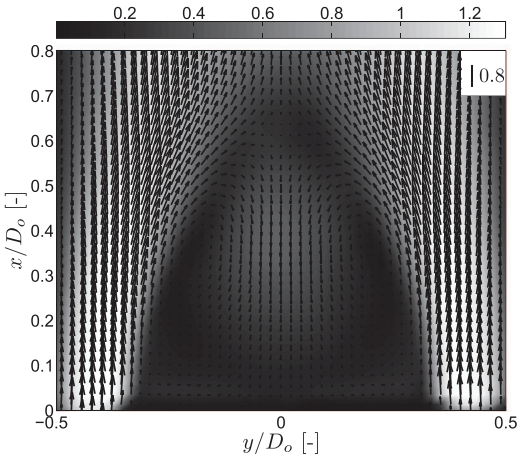

FIG. 7. Velocity vectors of the swirling jet ($|S| = 0.015$). The vectors are scaled with U_0. Colored according to magnitude.

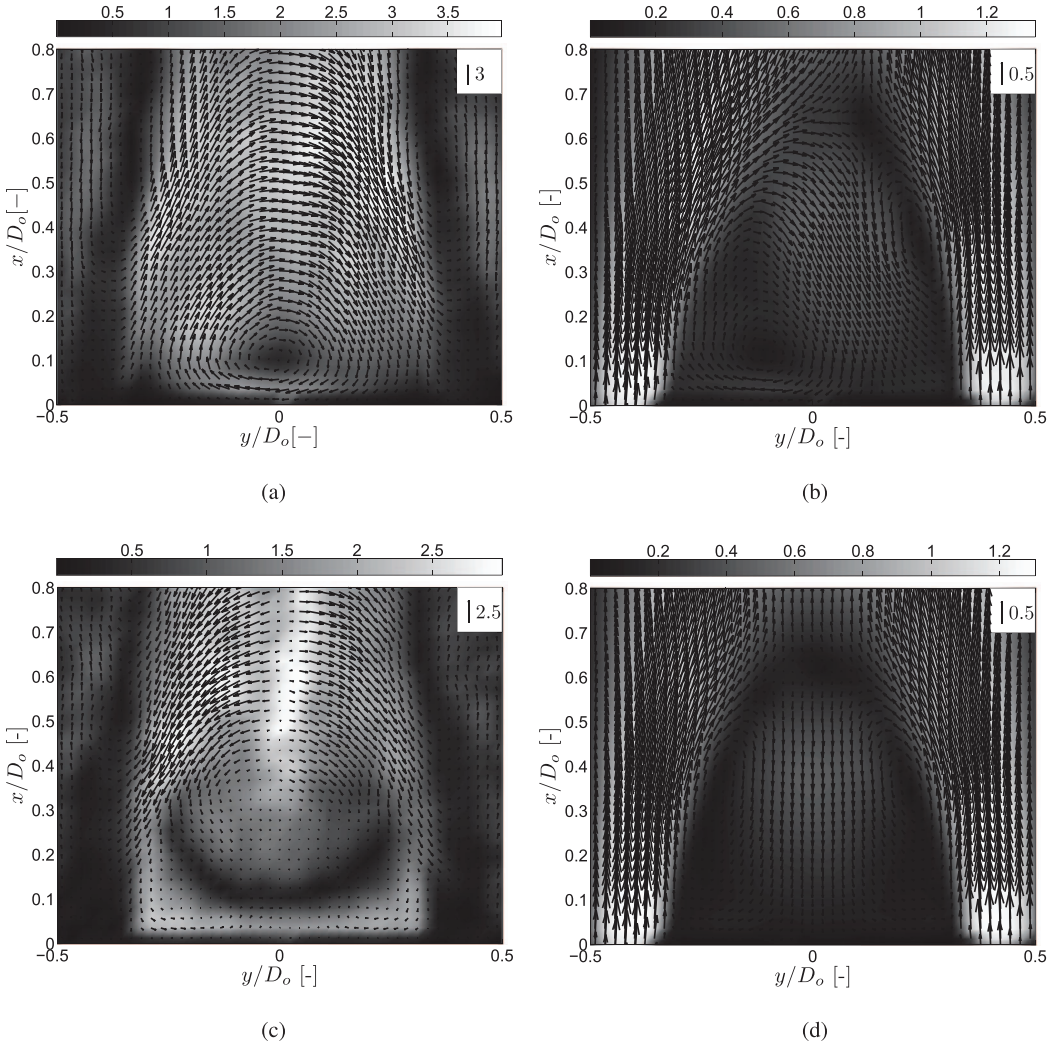

FIG. 8. Effect of the first two eigenmodes $a_1\overrightarrow{\psi}_1/U_0$ and $a_2\overrightarrow{\psi}_2/U_0$ on the flow field ($|S| = 0.015$). Data from a longitudinal measurement plane. Colored according to magnitude. Note: only one in four vectors is shown. (a) $\overrightarrow{\psi}_1/U_0$, (b) $\overrightarrow{U}/U_0 + \max_{\forall t}(a_1)\overrightarrow{\psi}_1/U_0$, (c) $\overrightarrow{\psi}_2/U_0$, (d) $\overrightarrow{U}/U_0 + \max_{\forall t}(a_2)\overrightarrow{\psi}_2/U_0$.

Despite the fact that the spatial eigenmodes of the non-swirling and swirling jet are very similar, the temporal reconstruction coefficients are very different. For the swirling jet ($|S| = 0.015$), the temporal reconstructions coefficients a_1 and a_2 are shown in Figs. 9(a) and 9(b). These coefficients are filtered in time with a low pass filter to remove the high frequency turbulent fluctuations. Unlike the non-swirling jet, looking at the frequency spectra (not shown here) shows the presence of a clear peak. For the third mode, a weak peak is present at double the precessing frequency and for the higher modes no clear peak can be found. For the non-swirling jet, these coefficients a_1 and a_2 were essentially uncorrelated, however, a cross-correlation of the data for the swirling jet shows that both coefficients are strongly correlated and a_2 is lagging a_1 by $\pi/2$ radians. Reconstruction of the velocity field shows that mode 1 and mode 2 represent a precession of the asymmetric wake around the central axis of the jet. This precession was also found in a study by Vanierschot and Van den Bulck.[19] In this paper, the 3D shape of the recirculation zone is reconstructed based on phase averaged data. In order to reveal the time aspects of the precession, Figs. 9(c) and 9(d) show the wavelet analyses of a_1 and a_2. The precession frequency is clearly present in the correlation

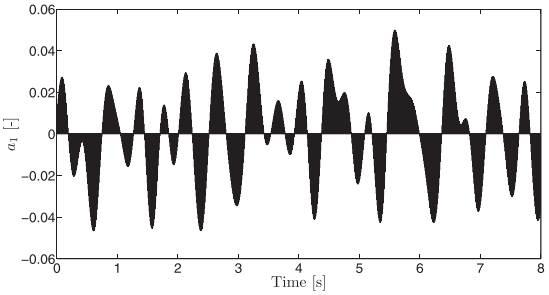

(a)

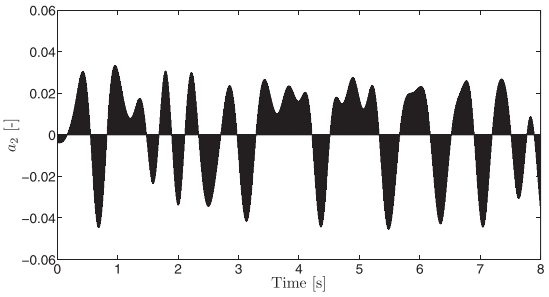

(b)

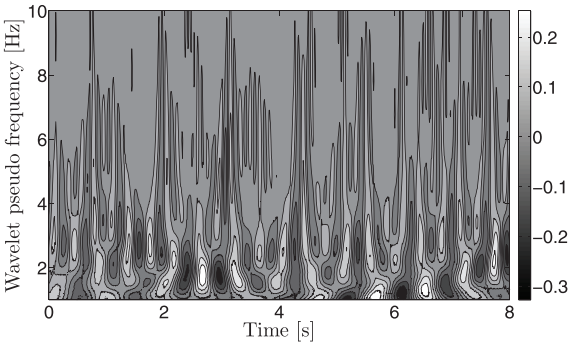

(c)

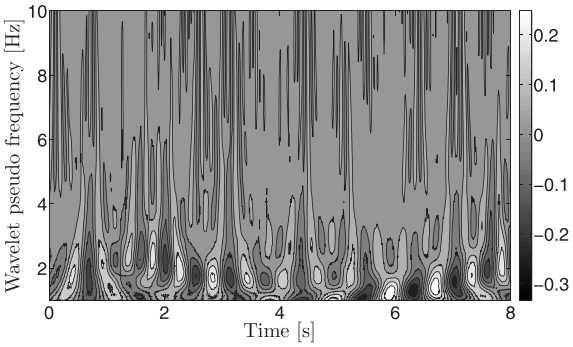

(d)

FIG. 9. Temporal reconstruction coefficients and their wavelet analysis for the swirling jet ($|S| = 0.015$). A Morlet wavelet is used in the decomposition. (a) First mode temporal reconstruction coefficient a_1, (b) second mode temporal reconstruction coefficient a_2, (c) wavelet decomposition of the first temporal coefficient a_1, (d) wavelet decomposition of the second temporal coefficient a_2.

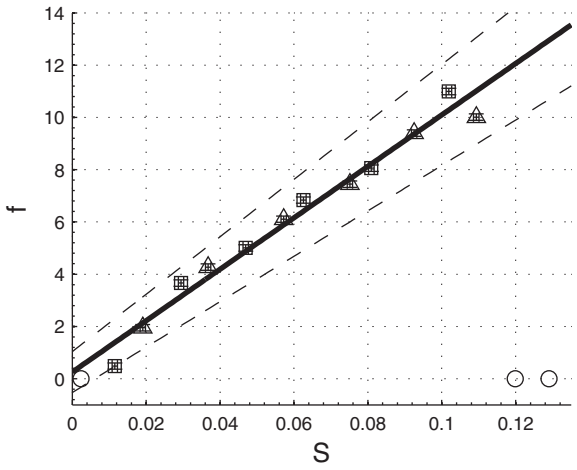

FIG. 10. Influence of the swirl number $|S|$ on the precession frequency f. Uncertainty on swirl number is due to PIV measuring error, while uncertainty on frequency is equal to Δf, the frequency resolution in the spectrum. Direction of swirl and rotation: $\triangle\ \theta\uparrow\ \square\ \theta\downarrow$. Measurements where precession is not detected are denoted by ◯. The linear regression of the data is denoted by the black line (the dashed lines give the 95% regression confidence-interval).

data. This precession frequency changes slightly in time due to turbulent fluctuations which alter the feedback mechanism of the stagnation point.

Since the spatial POD modes $\overrightarrow{\psi}_1$ and $\overrightarrow{\psi}_2$ for a swirling jet are very similar to the ones found in the zero swirl jet, swirl does not affect the asymmetric wake, it only makes its motion coherent into a single precession at selected frequencies. In order to test the hypothesis that the precession found by Vanierschot and Van den Bulck[19] for the non-swirling annular jet is swirl induced, the influence of swirl on the frequency f associated with the precession is studied. Analysis of the spectra for swirling jets in the range of $0 < |S| < 0.12$ shows clear peaks in the spectra of a_1 and a_2. This peak decreases in magnitude and spreads out to neighboring frequencies if the swirl number is increased, indicating a decay of the precession. Finally, for a swirl number outside the precession range ($|S| \geq 0.12$), no peak can be found in the spectrum. The relationship between f and $|S|$ is shown in Fig. 10. Clearly, the swirl number $|S|$ and the frequency f are closely linked and the relation is linear. The range of swirl numbers where the precession can be identified in the frequency spectrum goes up to $|S| \approx 0.11$ and hence the precession is confined to relatively low swirl numbers. The highest frequency found, (at $|S| \approx 0.11$), corresponds to a Strouhal number, based on the diameter of the bluff body D_i, equal to 0.013, which is still lower than the frequencies for shear layer instabilities found in literature. For $|S| = 0.002$ (zero swirl within measurement accuracy), no dominant frequency is present. As f and $|S|$ are closely linked, Fig. 10 suggests that swirl entrains the asymmetric wake and transforms the unstructured motion at zero swirl into a precession. Moreover, if the swirling direction is changed, the precession direction also changes. To derive a simple model for the influence of swirl on the precession, let us assume that the driving force for the precession is entrainment of the annular jet near the nozzle inlet at the base of the wake vortex. In a study by Del Taglia,[10] this was stated as the region where the perturbations originate and are convected towards the stagnation point, creating the asymmetric flow. The frequency-swirl relation can be derived by assuming that the asymmetric wake rotates with the same angular frequency as the jet and therefore there is no slip between the two. The radial profiles of W near the bluff body wall show this is a valid assumption. For a swirl number S, the average rotational velocity in the inlet channel can be estimated as $W_m = r\omega \approx U_m.S$, where ω is the angular frequency of rotation and hence also the rotational frequency of the wake. The frequency of precession is $f = \omega/2\pi$. Combining these two equations results in

$$f \approx \frac{U_m}{2\pi r_m} S = 105S, \tag{5}$$

with r_m is the mean radius of the channel. A linear regression of the data in Fig. 10 gives $f \approx 100|S|$ (black line in the figure). This observation, combined with the simple model of entrainment, indicates that for zero-swirl the precession is absent, implying that the precession phenomenon is driven by swirl. Moreover, the precession direction is the same as the swirl direction, e.g., if the swirl is changed in sign, the precession direction also changes.

As the POD analysis indicates, the wake for the swirling jet contains the same spatial structures as the non-swirling flow. Due to viscous entrainment of the swirling jet, these spatial structures move in a coordinated way at the frequency of the swirl. Hence, the relative amplitude for a swirling jet, $A_S(t)$, can be written as $A_S(t) = A(t) + \varepsilon \sin \omega t$, where $\varepsilon = 0.001$ is taken very small so that $A_S(t) \approx A(t)$ since these low swirl numbers have no significant influence on the structure of the wake. Substituting this expression into Eq. (3) results in

$$\frac{d}{dt}A(t) = \sigma A(t) - \mu |A_s(t-\tau)|^2 A(t) + \varepsilon[(\sigma - \mu |A_s(t-\tau)|^2) \sin \omega t - \omega \cos \omega t]. \quad (6)$$

This equation is the equivalent NLDS model for a swirling flow. The parameters σ and τ are dependent on the swirl number. Swirl induces pressure gradients in the radial direction, $\partial p/\partial r = \rho W^2/r$, which lower the pressure gradients in the axial direction at the central axis.[20] As a result, the convective feedback time τ increases linearly with increasing swirl. Also the perturbation growth rate is dependent on the swirl number as σ is irreversibly proportional to S. However, since the swirl numbers in this study are very low, the product $\sigma\tau \sim 3$, as is also the case for the non-swirling flow. Figure 11 shows the numerical simulation of Eq. (6) for a dimensionless swirling frequency $fT = 0.5$. Despite the very small value of ε, the chaotic behavior of the amplitude in Fig. 6 is now transformed into a structured motion. Since $\varepsilon = 10^{-3}$ is very small, the last term in Eq. (6) is only important at times where $A(t) \approx 0$. At these times, swirl sets the direction of the amplitude. In the frequency spectrum of the amplitude, a clear peak at the swirl frequency is present, together with smaller peaks at higher harmonics. As the swirl frequency is increased, these peaks remain in the spectra. The magnitude of the peaks however decreases with increasing swirl.

C. Flow structures for $S > 0.12$

Figure 12 shows the flow field of a swirling jet with swirl number $|S| = 0.16$. The wake becomes asymmetric, as is also observed by other studies.[20,34] As the swirl increases, a secondary vortex is formed near the bluff body wall because of pressure gradient reduction, imparted by swirl. With increasing swirl the negative pressure gradient at the central axis reduces, forcing the stagnation point at the wall to move downstream, creating the secondary vortex structure. This region is called the inverted triangle zone and this "triangle" increases with increasing swirl (more information can be found in the studies of Vanierschot and Van den Bulck[20] and Sheen *et al.*[34])

A POD analysis of the wake shows that only the first mode is clear enough to draw conclusions. The second and higher modes show no clear influence on the motion of the wake. The first eigenmode is shown in Fig. 13. It is very similar to the first modes for the low swirling jets ($0 \leq |S| < 0.12$) since the swirl induced pressure gradients in the axial direction at the central axis make the mode only slightly different near the bluff body wall. Like in the precious jets, this mode represents a motion of the wake in the measurement plane. Analysis of the corresponding temporal reconstruction coefficient, Fig. 14, shows that no well defined peak can be found in the spectra. Comparing a_1 with the corresponding non-swirling jet shows the swirling flow at $|S| = 0.16$ exhibits the same unstable behavior as for zero swirl. However, the wavelet coefficients are much smaller, indicating that the large scale motion of the wake becomes less pronounced.

Solving Eq. (6) for higher swirl numbers shows that at a frequency of $fT \approx 5.5$ and above, no clear peak in the spectrum can be found. Figure 15 shows the numerical simulation of Eq. (6) for $fT = 5.5$. The direction of the amplitude depends highly on the initial conditions and $A(t)$ shows the same behavior as for the non-swirling jet. Also the spectrum of $A(t)$ shows no clear peak at the swirling frequency. The period T can be calculated from Eq. (4). The convective time delay τ

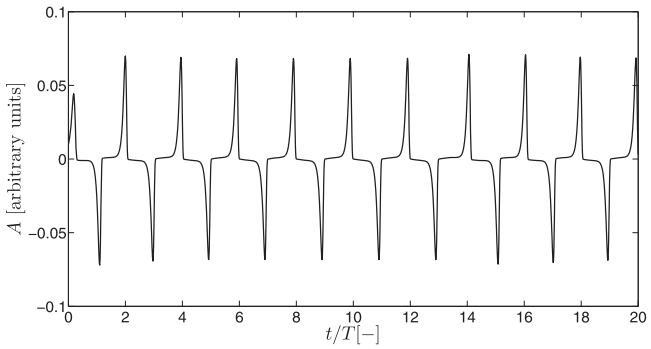

(a)

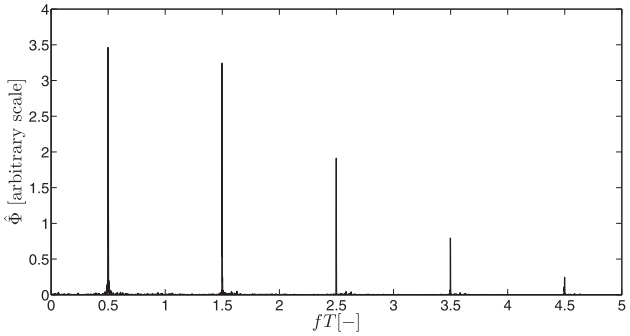

(b)

FIG. 11. Results of the numerical simulation of Eq. (6). The dimensionless feedback time $\tau = 3, \sigma\tau = 3$, and $\mu = 4000\sigma$. The dimensionless rotational frequency of the wake, scaled with T is 0.5. (a) Amplitude $A_S(t)$ as a function of the dimensionless time scaled with T. The amplitude is plotted in arbitrary units, (b) frequency spectrum of $A_S(t)$.

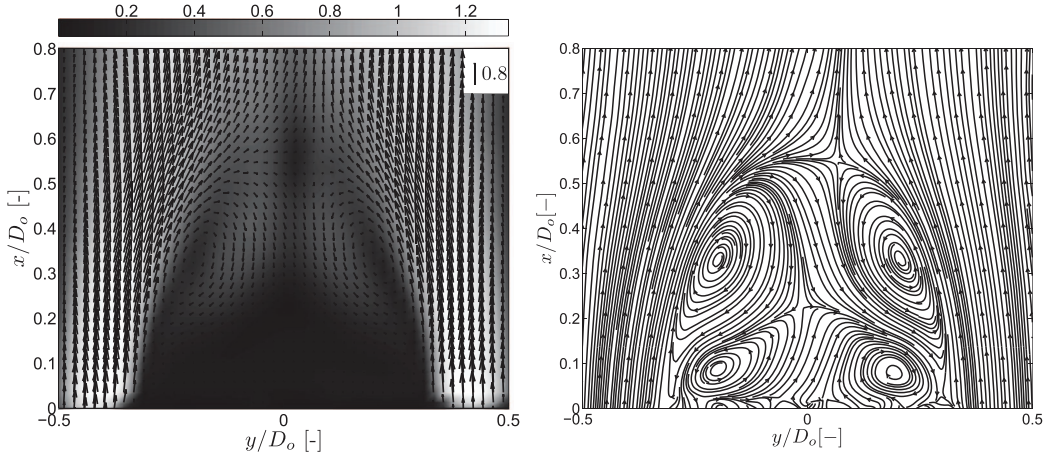

(a) (b)

FIG. 12. Flow field of the annular jet with swirl number $|S| = 0.16$. (a) Velocity vectors of the swirling jet. The vectors are scaled with U_0. Colored according to magnitude, (b) time averaged streamlines of the swirling jet.

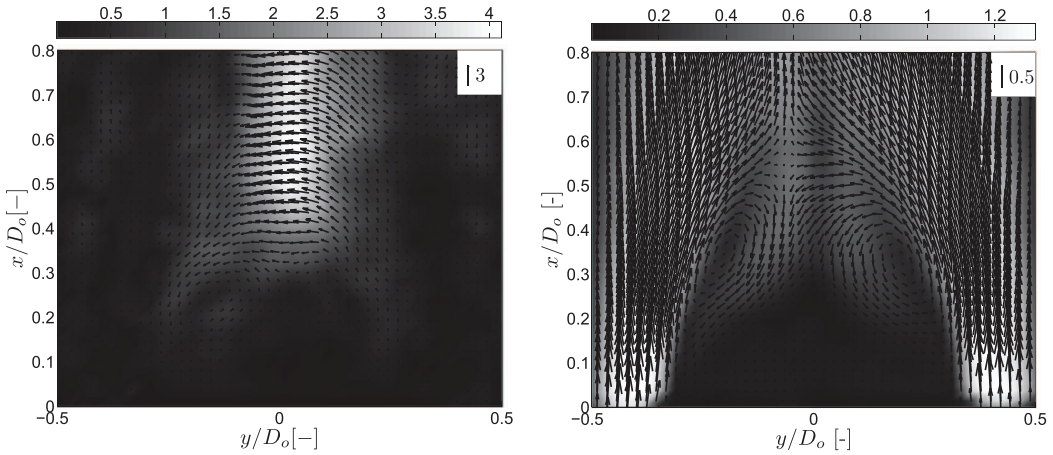

(a) (b)

FIG. 13. Effect of the first two eigenmodes $a_1\overrightarrow{\psi}_1/U_0$ and $a_2\overrightarrow{\psi}_2/U_0$ on the flow field ($|S| = 0.16$). Data from a longitudinal measurement plane. Colored according to magnitude. Note: only one in four vectors is shown. (a) $\overrightarrow{\psi}_1/U_0$, (b) $\overrightarrow{\overline{U}}/U_0 + \max_{\forall t}(a_1)\overrightarrow{\psi}_1/U_0$.

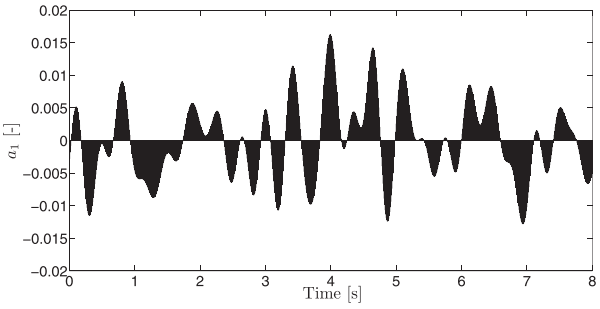

(a)

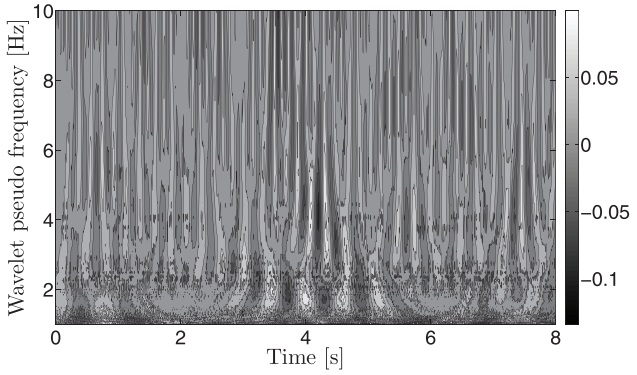

(b)

FIG. 14. Temporal reconstruction coefficients and their wavelet analysis for the swirling jet ($|S| = 0.16$). A Morlet wavelet is used in the decomposition. (a) First mode temporal reconstruction coefficient a_1, (b) wavelet decomposition of the first temporal coefficient a_1.

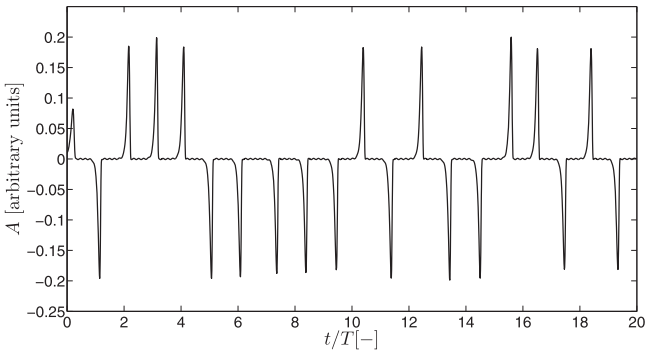

(a)

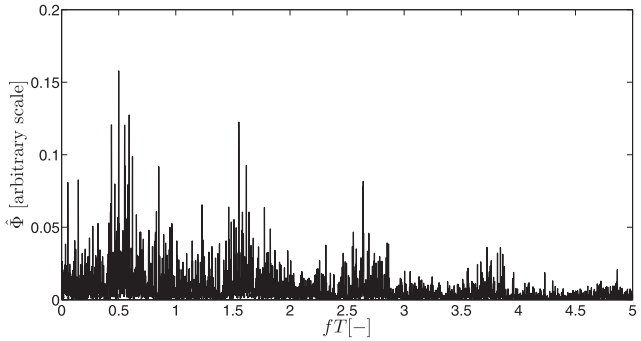

(b)

FIG. 15. Results of the numerical simulation of Eq. (3) for $S = 0.12$. The dimensionless feedback time $\tau = 3$, $\sigma\tau = 3$, and $\mu = 4000\sigma$. The dimensionless rotational frequency of the wake, scaled with T is 5.5. (a) Amplitude $A_S(t)$ as a function of the dimensionless time scaled with T. The amplitude is plotted in arbitrary units. (b) Frequency spectrum of $A_S(t)$.

for a swirling jet at $S = 0.12$ is 8 ms. Substituting this in Eq. (4) results in a period $T = 0.38$ s. Hence, the swirl frequency at which no peak can be found is equal to $5.5/T$ or 14.5 Hz. This is in close agreement with the results of the experiments, which give a highest frequency of around 11 Hz. Hence, the NLDS model with swirl is able to capture the dynamics of the wake motion and the influence of swirl on those dynamics.

IV. CONCLUSION

In this paper, a study is made of the bluff-body wake of a turbulent annular jet at very low swirl levels, ranging from 0 to 0.12. The flow field was measured using time-resolved PIV and analyzed using POD. It was shown that a large asymmetry of the wake vortex is present, which is also confirmed by other studies. The motion of the wake appears to be random in time and no coherent motion is present. When a very small amount of swirl is added to the jet, the motion of the asymmetric vortex is changed from randomly to a well defined precession at very low frequencies. This precession remains until a certain swirl number $|S| = 0.12$ is reached. At this swirl number, the motion of the asymmetric wake is not coordinated anymore and the same behavior occurs compared to the non-swirling wake. To simulate the physics of the flow field, a model was developed which assumes that the perturbations, which originate within the inner shear layer of the jet, close to the

bluff body wall, are entrained by swirl and create a coordinate motion between the jet and asymmetric wave through a convective feedback mechanism. A well known equation in literature to simulate this is the nonlinear delayed saturation model. In this study, the model is adapted for a swirling flow. With this model the dynamics of the wake could be simulated and comparison with experiments shows a good agreement.

ACKNOWLEDGMENTS

The authors gratefully acknowledge the funding of this work by the Fonds Wetenschappelijk Onderzoek (FWO) – Vlaanderen (Fund Scientific Research – Flanders).

[1] A. Gupta and G. Lilley, *Swirl Flows* (Abacus, Kent, 1984).
[2] J. Beér and N. Chigier, *Combustion Aerodynamics* (Krieger Pub. Co., 1983).
[3] J. Dugué and R. Weber, "Design and calibration of a 30 kW natural gas burner for the University of Michigan," Technical Report No. C74/y/1, IJmuiden, The Netherlands, 1992.
[4] J. Dugué and R. Weber, "Design and calibration of a 300 kW natural gas burner for berl," Technical Report C74/y/5, IJmuiden, The Netherlands, 1992.
[5] Y. M. Al-Abdeli and A. R. Masri, "Precession and recirculation in turbulent swirling isothermal jets," Combust. Sci. Technol. **176**, 645–665 (2004).
[6] M. García-Villalba and J. Frölich, "LES of free annular swirling jet-dependence of coherent structures on a pilot jet and the level of swirl," Int. J. Heat Fluid Flow **27**, 911–923 (2006).
[7] H. A. Warda, S. Z. Kassab, K. A. Elshorbagy, and E. A. Elsaadawy, "An experimental investigation of the near-field region of free turbulent round central and annular jets," Flow Meas. Instrum. **10**, 1–14 (1999).
[8] W. J. A. Dahm, C. E. Frieler, and G. Tryggvason, "Vortex structure and dynamics in the near field of a coaxial jet," J. Fluid Mech. **241**, 371–402 (1992).
[9] R. Sadr and J. C. Klewicki, "An experimental investigation of the near-field flow development in coaxial jets," Phys. Fluids **15**, 1233–1246 (2003).
[10] C. Del Taglia, L. Blum, J. Gass, Y. Ventikos, and D. Poulikakos, "Numerical and experimental investigation of an annular jet flow with large blockage," J. Fluid Eng. - Trans. ASME **126**(3), 375–384 (2004).
[11] C. Del Taglia, A. Moser, and L. Blum, "Spontaneous break of symmetry in unconfined laminar annular jets," J. Fluids Eng. - Trans. ASME **131**(8), 081202 (2009).
[12] N. W. M. Ko and W. T. Chan, "Similarity in initial region of annular jets - 3 configurations," J. Fluid Mech. **84**, 641–656 (1978).
[13] N. W. M. Ko and W. T. Chan, "Inner regions of annular jets," J. Fluid Mech. **93**, 549–584 (1979).
[14] W. T. Chan and N. W. M. Ko, "Coherent structures in the outer mixing region of annular jets," J. Fluid Mech. **89**, 515–533 (1978).
[15] D. F. G. Durão and J. H. Whitelaw, "Velocity characteristics of flow in near wake of a disk," J. Fluid Mech. **85**, 369–385 (1978).
[16] B. Patte-Rouland, G. Lalizel, J. Moreau, and E. Rouland, "Flow analysis of an annular jet by particle image velocimetry and proper orthogonal decomposition," Meas. Sci. Technol. **12**(9), 1404–1412 (2001).
[17] H. Rehab, E. Villermaux, and E. J. Hopfinger, "Flow regimes of large-velocity-ratio coaxial jets," J. Fluid Mech. **345**, 357–381 (1997).
[18] C. Duwig and E. Gutmark, "Large scale rotating motions in a multiple jets combustor," Phys. Fluids **20**(4), 041705 (2008).
[19] M. Vanierschot and E. Van den Bulck, "Experimental study of low precessing frequencies in the wake of a turbulent annular jet," Exp. Fluids **50**, 189–200 (2011).
[20] M. Vanierschot and E. Van den Bulck, "Influence of swirl on the initial merging zone of a turbulent annular jet," Phys. Fluids **20**(10), 105104 (2008).
[21] A. Melling, "Tracer particles and seeding for particle image velocimetry," Meas. Sci. Technol. **8**(12), 1406–1416 (1997).
[22] B. Wieneke, "Stereo-PIV using self-calibration on particle images," Exp. Fluids **39**(2), 267–280 (2005).
[23] J. Westerweek, "Efficient detection of spurious vectors in particle image velocimetry data," Exp. Fluids **16**(3–4), 236–247 (1994).
[24] R. J. Adrian, K. T. Christensen, and Z. C. Liu, "Analysis and interpretation of instantaneous turbulent velocity fields," Exp. Fluids **29**, 275–290 (2000).
[25] G. Berkooz, P. Holmes, and J. L. Lumley, "The proper orthogonal decomposition in the analysis of turbulent flows," Annu. Rev. Fluid Mech. **25**, 539–575 (1993).
[26] J. Kostas, J. Soria, and M. Chong, "A comparison between snapshot POD analysis of PIV velocity and vorticity data," Exp. Fluids **38**(2), 146–160 (2005).
[27] P. Holmes, J. L. Lumley, and G. Berkooz, *Turbulence, Coherent Structures, Dynamical Systems and Symmetry* (Cambridge University Press, 1996).
[28] M. Vanierschot, K. Van Dyck, and E. Van den Bulck, "A comparison of large scale extraction methods in the study of annular wake flow," Flow, Turbul. Combust. **91**(1), 63–77 (2013).
[29] E. Villermaux and E. J. Hopfinger, "Periodically arranged co-flowing jets," J. Fluid Mech. **263**, 63–92 (1994).

[30] E. Villermaux and E. J. Hopfinger, "Self-sustained oscillations of a confined jet: A case-study for the nonlinear delayed saturation model," Physica D **72**(3), 230–243 (1994).
[31] G. K. Batchelor and A. E. Gill, "Analysis of the stability of axisymmetric jets," J. Fluid Mech. **14**, 529–551 (1962).
[32] A. Michalke, "Survey on jet instability theory," Prog. Aerospace Sci. **21**, 159–199 (1984).
[33] L. F. Shampine and S. Thompson, "Solving DDEs in Matlab," Appl. Numer. Math. **37**, 441–458 (2001).
[34] H. Sheen, W. Chen, and S. Jeng, "Recirculation zones of unconfined and confined annular swirling jets," AIAA J. **34**, 572–579 (1996).